

Fourier transform spectroscopy of d -wave quasiparticles in the presence of atomic scale pairing disorder

Tamara S. Nunner,* Wei Chen, Brian M. Andersen, Ashot Melikyan, and P. J. Hirschfeld
Department of Physics, University of Florida, Gainesville, Florida 32611, USA

(Received 5 September 2005; revised manuscript received 1 December 2005; published 23 March 2006)

The local density of states power spectrum of optimally doped $\text{Bi}_2\text{Sr}_2\text{CaCu}_2\text{O}_{8+x}$ (BSCCO) has been interpreted in terms of quasiparticle interference peaks corresponding to an “octet” of scattering wave vectors connecting \mathbf{k} points where the density of states is maximal. Until now, theoretical treatments have not been able to reproduce the experimentally observed weights and widths of these octet peaks; in particular, the predominance of the dispersing “ \mathbf{q}_1 ” peak parallel to the Cu-O bond directions has remained a mystery. In addition, such theories predict “background” features which are not observed experimentally. Here, we show that most of the discrepancies can be resolved when a realistic model for the out-of-plane disorder in BSCCO is used. Weak extended potential scatterers, which are assumed to represent cation disorder, suppress large-momentum features and broaden the low-energy “ \mathbf{q}_7 ” peaks, whereas scattering at order parameter variations, possibly caused by a dopant-modulated pair interaction around interstitial oxygens, strongly enhances the dispersing \mathbf{q}_1 peaks.

DOI: [10.1103/PhysRevB.73.104511](https://doi.org/10.1103/PhysRevB.73.104511)

PACS number(s): 74.40.+k, 74.25.Bt, 74.25.Jb

I. INTRODUCTION

For several years, high-resolution scanning tunneling microscopy (STM) experiments^{1–14} have been imaging the local electronic structure of cuprate superconductors. These experiments have discovered resonant defect states^{1–3} and revealed the existence of nanoscale inhomogeneities.^{4–7} From a highly disordered spatial tunneling signal, it has become standard to use Fourier transform scanning tunneling spectroscopy¹⁵ (FT-STs) techniques to extract, e.g., the characteristic wavelengths of Friedel-type oscillations¹⁶ and, if present, the background charge order. In a simple metal, the local density of states around an impurity varies as $\sim \cos 2k_F r/r^3$, so the wavelength of the local density of states (LDOS) “ripples” caused by a single impurity is a measure of the Fermi wave vector of the pure system.¹⁵ In the quasi-two-dimensional (2D) d -wave superconductor, the spherical shell of maximum FT-STs intensity with radius $2k_F$ is replaced by a discrete set of peaks at positions \mathbf{q}_α , $\alpha = 0, \dots, 7$ (see Fig. 1) which connect an octet of points of high density of states in momentum space.^{8,17–21} The fact that in optimally doped BSCCO the measured dispersion of these peaks with STM bias^{8,12,13} agrees semiquantitatively with the predictions based on d -wave BCS theory is considered as strong evidence for the existence of well-defined quasiparticles in the superconducting state of optimally doped cuprate superconductors, and for the applicability of d -wave BCS theory in this regime. Recent attempts to relate ARPES spectral functions to STM Fourier transform patterns have met with reasonable success, supporting this conclusion.^{22–24}

At lower doping, the dispersing peaks are still present, but additional nondispersing peaks are observed corresponding to wave vectors along the Cu-O bonds with wavelength close to four lattice spacings.^{13,14} Nondispersing peaks have been reported in overdoped samples as well, and have been discussed in terms of stripelike charge ordering.^{9,10} The nature and degree of charge ordering and the existence of the non-

dispersive peaks in these materials is still controversial, however. In this work we neglect charge ordering and discuss exclusively the Fourier transform LDOS response of the d -wave superconducting state to disorder.

Despite the overall success of interpreting the Fourier STM patterns in terms of quasiparticle interference, none of the existing models has been able to correctly account for the observed weights and widths of the dispersive q -space peaks. The pointlike single-impurity theories^{8,17–21} yield peak structures which are sharp, and linear or arclike in structure, in contrast to the experimental features, which appear as a series of broad, roughly round spots. Depending on the assumed form of the impurity potential and its strength, the relative intensity weights of the different octet peaks change,

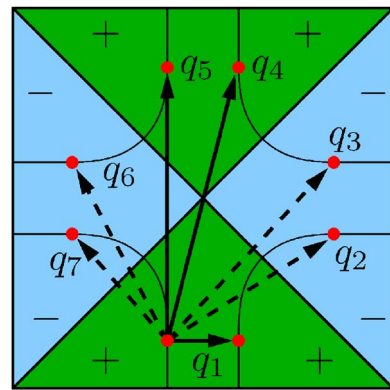


FIG. 1. (Color online). Schematic depiction of the first Brillouin zone in cuprate superconductors. Green (dark gray) and blue (light gray) regions represent $\Delta_{\mathbf{k}} > 0$ and $\Delta_{\mathbf{k}} < 0$, respectively. Red (gray) dots are intersections of constant quasiparticle energy contours with the Fermi surface. The fraction of octet vectors, \mathbf{q}_1 , \mathbf{q}_4 , \mathbf{q}_5 which should in principle be visible in the case of a “pointlike” (four bond) order parameter modulation (τ_1 scatterer) are denoted with solid lines. The remaining octet vectors are indicated with dashed lines.

but there has been no choice of potential found which adequately accounts for the experimentally observed weights. In particular, all such calculations appear to drastically underestimate the weight of the dispersing \mathbf{q}_1 peaks and in contrast to experiment predict many “background” features, i.e., strong intensity in regions of q space other than the octet peaks.

Many-impurity calculations with weak scatterers displayed some of the same features as the single-impurity calculations, and showed how increasing disorder eventually swamps the octet peaks by raising the noise floor, but were not notably more successful in reproducing the experimental FT-STS patterns.²⁵ It was therefore suggested by Zhu *et al.*²⁶ that it is essential to consider a more realistic disorder model for BSCCO, including the effect of roughly 0.2% in-plane native defects, which are generally considered as strong pointlike scatterers due to the resonances they generate near zero bias,¹¹ as well as the effect of out-of-plane defects, which most likely act as weak extended scatterers due to poor screening within the CuO_2 planes. Using this disorder model Zhu *et al.* were able to reproduce the experimental FT-STS patterns at low biases of order 10–15 meV reasonably well, but at higher energies agreement was rather poor. They attributed the low-energy behavior to the in-plane native defects and interpreted the role of the extended weak out-of-plane scatterers as broadening the octet peaks. They noted in addition the weakness of the \mathbf{q}_1 octet peak produced by their model in the intermediate energy range. A broadening of small-momentum features and enhancement of \mathbf{q}_1 scattering was also reported by Dell’Anna *et al.*²⁷ due to assumed nanoscale order parameter inhomogeneities, and similar results were obtained very recently by Su and Cheng.²⁸

In this paper we show that a realistic treatment of the out-of-plane disorder plus the consideration of in-plane native defects is necessary to understand the key features of the experimental Fourier transform patterns. There are at least two major sources of out-of-plane disorder in this material: (i) nonstoichiometric oxygen dopant atoms and (ii) random substitution of Bi at the Sr sites.²⁹ Very recently, direct information on both types of impurities has been obtained by STM. Kinoda *et al.*³⁰ succeeded in imaging the excess Bi^{3+} at a bias of 1.7 eV, finding an areal concentration of about 3%, consistent with earlier estimates from bulk measurements.²⁹ In addition, McElroy *et al.*³¹ imaged a set of atomic scale defects at -0.96 eV, whose concentration scales with doping. These defects, which were ultimately identified as the interstitial oxygen dopant atoms, were shown to correlate strongly and positively with the local gap size in the superconducting state.

We have recently suggested that the results of Ref. 31 can be understood based on the simple assumption that the main effect of the interstitial dopants [i.e., disorder (i)] is to increase the pair interaction locally.³² This assumption yields gap modulations which correlate positively with the dopant positions, gives rise to particle-hole symmetric spectra and suppresses high-energy coherence peaks as observed in experiment. The idea of a modulated pair interaction has been raised before, e.g., in the context of the formation of local superconductivity near impurities^{33,34} and the modulation of

the pair interaction near twin boundaries.³⁵ As a first step towards a microscopic picture of how the dopants could modulate the pair interaction, we have recently performed an *ab initio* calculation for BSCCO-2212 including an additional oxygen interstitial.³⁶ One of the main results is that the oxygen interstitial deforms the lattice strongly, including a large displacement of the apical oxygen. This could be of relevance since the distance of the apical oxygen to the CuO_2 planes has been speculated to affect the magnitude of the superconducting transition temperature.^{37,38}

The determination of the local distortions of the stoichiometric positions of atoms near the CuO_2 plane can in principle be used to recalculate the coupling of electrons to collective excitations of the ionic and electronic system which lead to pairing. One possibility for a microscopic picture is that the superexchange between electrons on the Cu sites, frequently assumed to give rise to pairing in magnetically based theories of high T_c , is modulated locally. It is known from magnetic susceptibility experiments under pressure that the superexchange J in La_2CuO_4 varies as roughly the sixth power of the Cu-Cu distance.³⁹ Using this result it is easy to estimate that a change in lattice constant of order a few percent is sufficient to change J by an amount 30% sufficient to produce the gap modulations of Ref. 31 within the phenomenological proposal of impurity-modulated pair disorder,³² if J is identified as the scale of the pairing interaction. Very recently, Zhu adopted this microscopic picture and explored the effect of dopant modulated Cu-Cu hopping, which strictly determines a modulated J , within a Bogoliubov-de Gennes framework.⁴²

In the case of lattice vibrations, the local lattice distortions could modulate the electron-phonon coupling to some of the phonon modes. This has been discussed in the context of the Fourier patterns observed in inelastic tunneling spectroscopy (IETS),⁴³ where several candidate phonon modes were considered. While this work does not yet conclusively identify the mode responsible for pairing, it does strongly suggest that some mode has been observed and is strongly correlated with the *local* superconducting gap. At present the most promising comparison to experiment has been obtained with the B_{1g} “buckling” phonon mode, which is known to give rise to pairing of $d_{x^2-y^2}$ symmetry. A more convincing picture within this analysis is actually obtained when one assumes that the disorder required to observe the FT-IETS patterns is of the off-diagonal type considered here.⁴⁴

Although order parameter modulations could also arise from other sources, e.g., via coupling of ordinary electrostatic impurity potentials to phases which compete with d -wave superconductivity, see, e.g., Ref. 40, our phenomenological assumption of microscopic pairing disorder has already proven successful with respect to many experimental observations in BSCCO. Scattering by order parameter variations has been reported to improve dramatically the fit to the inelastic tunneling spectroscopy experiments.⁴⁴ Fang *et al.*⁴¹ reported very sharp coherence peaks in small gap regions consistent with an Andreev bound state in a region of suppressed order parameter, as discussed in Ref. 32. Finally, order parameter modulations with a phase twist have been found to yield low-energy impurity bound state energies and a spatial distribution of the LDOS similar to those observed

near Zn impurities in BSCCO-2212.⁴⁵ Thus it is intriguing to explore the consequences of this unusual quasiparticle scattering from the order parameter modulations further, in particular its effect on the FT-STS patterns.

Unlike the oxygen dopants, the Bi^{3+} defects, i.e., disorder component (ii), most likely act as conventional weak and extended potential scatterers due to the different charge of the Sr and Bi ions and the smaller deformation of the lattice itself. The existence of a large concentration of extended weak potential scatterers is also supported by an analysis of transport properties in BSCCO.⁴⁶

The final aspect of the disorder we discuss is the small concentration of in-plane native defects, about 0.2% per Cu, as imaged by the STM.¹¹ It is believed that these are Cu vacancies in the CuO_2 plane, although no direct proof exists. Individually, these defects provide a resonant signal centered within 1 meV of the Fermi level similar but not identical to Zn. The resonance modulates the LDOS primarily below 15 meV or less, and then furthermore at energies not far from the gap edge where the resonant spectral weight originates. We model these defects as strong pointlike unitary potential scatterers, as in Zhu *et al.*,²⁶ noting that because the concentration and resonance energies of these defects are known from experiment, they do not introduce new model parameters.

Thus, we propose that a realistic model of the disorder in BSCCO should contain a net out-of-plane disorder consisting of extended weak potential scatterers (approximately 3%, i.e., the concentration of Bi defects) and extended off-diagonal scatterers (approximately 7.5%, i.e., half the doping, because each oxygen dopant most likely contributes two holes) plus a concentration of 0.2% pointlike and strong in-plane defects. It is the purpose of this paper to investigate the effect of these three disorder components on the FT-STS patterns.

II. MODEL

As a model for the homogeneous system we use the usual BCS Hamiltonian given by

$$\mathcal{H}_0 = \sum_{\mathbf{k}, \sigma} \varepsilon_{\mathbf{k}} \hat{c}_{\mathbf{k}\sigma}^\dagger \hat{c}_{\mathbf{k}\sigma} + \sum_{\mathbf{k}} (\Delta_{\mathbf{k}} \hat{c}_{\mathbf{k}\uparrow}^\dagger \hat{c}_{-\mathbf{k}\downarrow}^\dagger + \text{H.c.}), \quad (1)$$

where $\varepsilon_{\mathbf{k}}$ is the quasiparticle dispersion proposed to fit the angle-resolved photoelectron spectroscopy (ARPES) data:⁴⁷ $\varepsilon_{\mathbf{k}} = \sum_{n=0}^5 t_n \chi_n(k)$, where $t_{0-5} = 0.1305, -0.5951, 0.1636, -0.0519, -0.1117, 0.0510$ (eV), and $\chi_{0-5}(k) = 1, (\cos k_x + \cos k_y)/2, \cos k_x \cos k_y, (\cos 2k_x + \cos 2k_y)/2, (\cos 2k_x \cos k_y + \cos 2k_y \cos k_x)/2$, and $\cos 2k_x \cos 2k_y$. For d -wave pairing we have, $\Delta_{\mathbf{k}} = 2\Delta_0(\cos k_x - \cos k_y)$ with $\Delta_0 = 12$ meV and we adopt the lattice spacing a as our length unit.

In terms of the Nambu spinor $\hat{\psi}_{\mathbf{k}}^\dagger = (\hat{c}_{\mathbf{k}\uparrow}^\dagger, \hat{c}_{-\mathbf{k}\downarrow}^\dagger)$, the corresponding bulk Green's function in Matsubara representation is given by

$$\mathcal{G}^0(\mathbf{k}, i\omega_n) = \frac{i\omega_n \tau_0 + \xi_{\mathbf{k}} \tau_3 + \Delta_{\mathbf{k}} \tau_1}{(i\omega_n)^2 - E_{\mathbf{k}}^2}, \quad (2)$$

where $E_{\mathbf{k}}^2 = \xi_{\mathbf{k}}^2 + \Delta_{\mathbf{k}}^2$, and τ_0 is the 2×2 identity matrix, whereas (τ_1, τ_2, τ_3) denote the three Pauli matrices. In real space, the perturbation due to the conventional potential scatterers in the diagonal τ_3 channel and modulated pairing amplitude in the off diagonal τ_1 channel can be written as

$$\mathcal{H}'(\mathbf{r}, \mathbf{r}') = \hat{\psi}_{\mathbf{r}}^\dagger [V(\mathbf{r}) \delta(\mathbf{r} - \mathbf{r}') \tau_3 + \delta\Delta(\mathbf{r}, \mathbf{r}') \tau_1] \hat{\psi}_{\mathbf{r}'}. \quad (3)$$

Note that the conventional impurity scattering occurs with Pauli matrix τ_3 in (3), whereas the order parameter modulation, or Andreev scattering term, occurs with τ_1 . We will henceforth adopt the convenient shorthand of referring to the two types of processes as τ_3 or τ_1 disorder, respectively.

The conventional τ_3 disorder

$$V(\mathbf{r}) = V_s \delta(\mathbf{r}) + V_{\text{ext}}(\mathbf{r}) \quad (4)$$

contains the potential of the pointlike strong in-plane defects V_s and the extended potential of the out-of-plane defects V_{ext} which we model with a Yukawa form as

$$V_{\text{ext}}(\mathbf{r}) = V_0 \frac{e^{-(d-r_z)/\lambda}}{d/r_z} \quad \text{with } d = \sqrt{r^2 + r_z^2}, \quad (5)$$

where \mathbf{r} is an in-plane vector, r_z is the distance of the defect from the CuO_2 plane, and the potential is normalized to V_0 in the CuO_2 plane directly below the defect.

A "pointlike" τ_1 scatterer corresponds to the modulation of the order parameter on the four bonds surrounding the impurity site as $\delta\Delta(0, \pm\hat{x}) = \delta\Delta(\pm\hat{x}, 0) = -\delta\Delta(0, \pm\hat{y}) = -\delta\Delta(\pm\hat{y}, 0) = \delta\Delta$ and an extended τ_1 scatterer is modeled with the same form as the τ_3 case

$$\delta\Delta(\mathbf{r}, \mathbf{r}') = \delta\Delta \frac{e^{-(d-r_z)/\lambda}}{d/r_z} \quad \text{with } d = \sqrt{\left[\frac{1}{2}(\mathbf{r} + \mathbf{r}')\right]^2 + r_z^2}, \quad (6)$$

simply because the exact functional form of the order parameter modulation is not known. We note that there is no implied microscopic origin of this form, nor any direct connection with a physical screened Coulomb potential; this is merely a convenient way for us to introduce a length scale to the order parameter modulations induced by the dopant atoms. Our disorder model combines the most important aspects of the actual disorder in BSCCO: the presence of extended potential out-of-plane scatterers, the presence of order parameter modulations caused by the oxygen dopant atoms and the existence of native defects which act as strong pointlike in-plane scatterers. Although we do not know the exact functional form of the order parameter modulations we consider the model "realistic" because it combines these different disorder components, whereas previous treatments have mostly focused on a single disorder component, and therefore were not able to span the full energy range of experimental observation.

In order to determine the resulting LDOS as a function of energy and lattice sites, one needs to obtain the full Green's function $\mathcal{G}(\mathbf{r}, \mathbf{r}', i\omega_n)$ given by the Dyson equation

$$\mathcal{G}(\mathbf{r}, \mathbf{r}') = \mathcal{G}^0(\mathbf{r} - \mathbf{r}') + \sum_{\mathbf{r}'', \mathbf{r}'''} \mathcal{G}^0(\mathbf{r} - \mathbf{r}'') \mathcal{H}'(\mathbf{r}'', \mathbf{r}''') \mathcal{G}(\mathbf{r}''', \mathbf{r}'). \quad (7)$$

Thus, by calculating

$$\mathcal{G}^0(\mathbf{r}, i\omega_n) = \sum_{\mathbf{k}} \frac{(i\omega_n \tau_0 + \xi_{\mathbf{k}} \tau_3 + \Delta_{\mathbf{k}} \tau_1)}{(i\omega_n)^2 - E_{\mathbf{k}}^2} \exp(i\mathbf{k} \cdot \mathbf{r}), \quad (8)$$

the remaining problem is that of a simple matrix inversion, and the LDOS $\rho(\mathbf{r}, \omega)$ can be extracted from the imaginary part of the full Green's function, $\rho(\mathbf{r}, \omega) = -\frac{1}{\pi} \text{Im } \mathcal{G}_{11}(\mathbf{r}, \mathbf{r}, \omega)$.

III. RESULTS

We now examine the effect of a single scatterer on the FT-STs patterns. The philosophy of calculations of this type^{17,18} is simply that the ‘‘Friedel oscillations’’ in the d -wave quasiparticle sea around a single impurity will contain many of the wavelengths present in the fully disordered system. The FTDOS due to the impurity is then given by

$$\rho(\mathbf{q}, \omega) = \sum_{\mathbf{r} \in L \times L} e^{-i\mathbf{q} \cdot \mathbf{r}} \rho(\mathbf{r}, \omega), \quad (9)$$

where $L \times L$ is a square set of L^2 positions at which measurements are made, and $\mathbf{q} = 2\pi(m, n)/L$ are vectors in the associated reciprocal lattice. The power spectrum⁴⁸ is simply the 2D image obtained from the amplitude $|\rho(\mathbf{q}, \omega)|$. In the case that several disorder components are present we calculate the power spectrum as $|\rho(\mathbf{q}, \omega)| = |\sum_i n_i \rho_i(\mathbf{q}, \omega)|$, where ρ_i and n_i denote the FTDOS and concentration of each disorder component.

Figure 2 compares the resulting power spectra for different impurity models computed for $L=53$. In the first column, the power spectrum for a weak pointlike τ_3 impurity, discussed previously in Refs. 18 and 26, is reproduced. In contrast to the experimental power spectrum, the calculation for a pointlike τ_3 impurity predicts strong weight at large wave vectors especially near (π, π) , which is observed experimentally only at very low frequencies. In the case of an extended τ_3 scatterer (second column in Fig. 2), on the other hand, the high-momentum features are suppressed due to the rapid falloff of the impurity potential $V(\mathbf{q})$ in momentum space. This is, however, not the only difference between pointlike and extended τ_3 scatterers. The FT patterns also change for small momenta; most noticeably, the \mathbf{q}_7 peaks are enhanced due to small-angle scattering of quasiparticles by the smooth potential. Whereas the \mathbf{q}_7 peaks appear only as tiny spots in the case of a pointlike impurity,²⁶ too small to be resolved in Fig. 2, they become broad spots in the case of an extended impurity and are clearly visible at the energies $|\omega| = 14$ meV, 22 meV in Fig. 2. This supports the proposal by Zhu *et al.*²⁶ that the enhancement of forward scattering due to spatially extended impurities broadens the octet peaks.

In addition to the existence of weak extended τ_3 scatterers, which could arise, e.g., due to random substitutions of Sr by Bi, the pair interaction is most likely modulated due to the

presence of nonstoichiometric oxygen dopant atoms.³² This results in inhomogeneities in the magnitude of the superconducting order parameter and enhanced Andreev scattering which can be modeled as τ_1 scattering within a single-impurity approach. The third column in Fig. 2 shows the power spectrum for a ‘‘pointlike’’ τ_1 scatterer, i.e., a modulation of the order parameter on the four bonds surrounding the impurity site as $\delta\Delta(0, \pm\hat{x}) = \delta\Delta(\pm\hat{x}, 0) = -\delta\Delta(0, \pm\hat{y}) = -\delta\Delta(\pm\hat{y}, 0) = \delta\Delta$. Obviously, the resulting FT pattern looks very different from a pointlike τ_3 scatterer. The background features, i.e., the finite FTDOS at wave vectors that do not correspond to one of the octet peaks, are much less pronounced. At high energies ($|\omega| = 30$ meV, 38 meV), the power spectrum is clearly dominated by \mathbf{q}_1 peaks, whereas the \mathbf{q}_7 peaks are completely absent even at the lowest energies. This behavior can be understood in terms of the momentum dependence of the scattering matrix element for a pointlike τ_1 scatterer. Fourier transformation of the pointlike order parameter modulation yields

$$\delta\Delta_{\mathbf{k}\mathbf{k}'} = \delta\Delta(\Delta_{\mathbf{k}} + \Delta_{\mathbf{k}'})/\Delta_0, \quad (10)$$

i.e., $\delta\Delta_{\mathbf{k}\mathbf{k}'}$ vanishes for wave vectors \mathbf{k} and \mathbf{k}' which connect points of the Brillouin zone where $\Delta_{\mathbf{k}}$ and $\Delta_{\mathbf{k}'}$ have opposite signs but equal magnitudes. Among the octet vectors, only \mathbf{q}_1 , \mathbf{q}_4 , and \mathbf{q}_5 are allowed scattering processes contributing to the FTDOS for a pointlike τ_1 scatterer, whereas \mathbf{q}_2 , \mathbf{q}_3 , \mathbf{q}_6 , and \mathbf{q}_7 are suppressed because the matrix element $\delta\Delta_{\mathbf{k},\mathbf{k}'}$ vanishes for these \mathbf{q} , see Fig. 1. The fourth column of Fig. 2 shows the power spectrum for the case of a slightly more extended τ_1 scatterer. The primary effect of extending the spatial range of the order parameter modulation is analogous to the τ_3 case, i.e., the intensity at large momenta and background features are suppressed resulting in even more pronounced \mathbf{q}_1 peaks.

The fifth column of Fig. 2 presents the power spectrum of an extended impurity with a combined τ_1 plus τ_3 potential, where each single component corresponds to the potential used for the extended τ_3/τ_1 case in the second/fourth column. Since we assume that the extended τ_3 scatterers result from the 3% Sr/Bi disorder and the extended τ_1 scatterers from the 7.5% dopant oxygens the FTDOS of each component has been weighted with a prefactor corresponding to the ratio of these two concentrations. Alternatively, a scatterer with combined τ_1 and τ_3 character could also arise due to the fact that each oxygen dopant, besides modulating the pair potential, most likely also possesses a small but finite conventional potential component. The extended $\tau_1 + \tau_3$ case obviously combines the main characteristics of the extended τ_1 and the extended τ_3 case. At $|\omega| = 14$ meV the power spectrum is dominated by \mathbf{q}_7 peaks, at $|\omega| = 22$ meV both the \mathbf{q}_7 and the \mathbf{q}_1 peaks are present, whereas the highest frequencies $|\omega| = 30$ meV and $|\omega| = 38$ meV are clearly dominated by \mathbf{q}_1 peaks.

In addition to out-of-plane impurities, a realistic description of the disorder in BSCCO has to take into account the in-plane native defects with concentration estimated as 0.2% from the STM. These defects are usually modeled as pointlike unitary impurities located within the CuO_2 planes. The

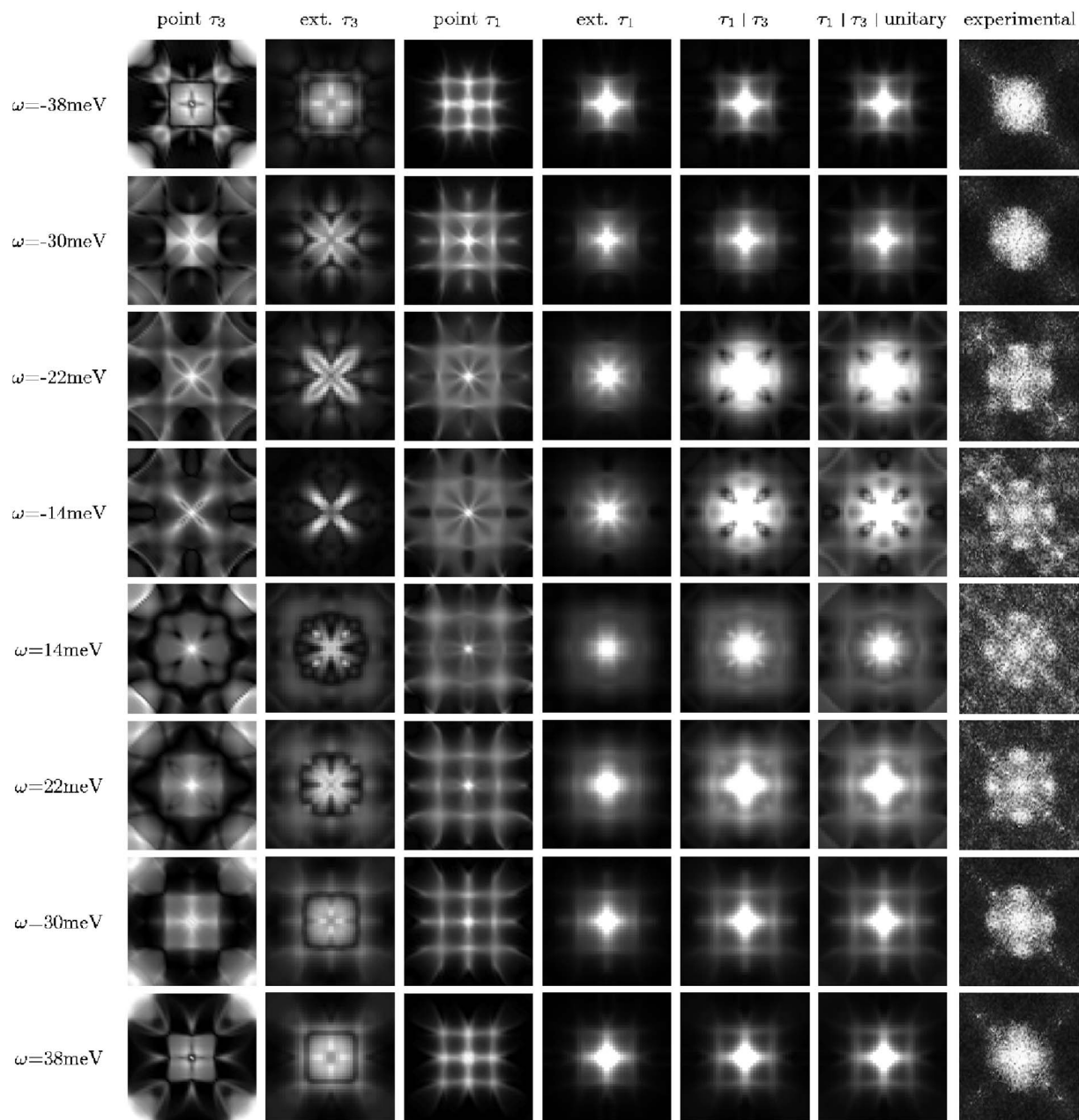


FIG. 2. Effect of out-of-plane scattering potentials of different type on the power spectrum. The power spectrum is shown for: first column: pointlike τ_3 scatterer with strength $V_s=120$ meV, second column: extended τ_3 scatterer with $V_0=40$ meV, $\lambda=r_z=1.5$, third column: pointlike τ_1 scatterer with $\delta\Delta=\Delta_0$ on the four central bonds, fourth column: slightly extended τ_1 scatterer with $\delta\Delta=\Delta_0$, $\lambda=r_z=1.2$, fifth column: combination of 7.5% extended τ_1 scatterers ($\delta\Delta=\Delta_0$, $\lambda=r_z=1.2$) and 3% extended τ_3 scatterers ($V_0=40$ meV, $\lambda=r_z=1.5$), sixth column: same as fifth column plus 0.2% unitary ($V_s=3.9$ meV) pointlike scatterers, seventh column: experimental power spectrum (Refs. 12 and 13).

sixth column of Fig. 2 displays the power spectrum resulting from the combined effect of the extended τ_1 and τ_3 scatterers, as displayed in the fifth column of Fig. 2, plus 0.2% pointlike unitary impurities (here $V_s=3.9$ eV). The existence of native defects within the CuO_2 planes of BSCCO is only of minor importance for the high-frequency power spectrum, because their concentration is much smaller than that of the out-of-plane defects. At smaller frequencies, however, the strong pointlike impurities produce additional large-momentum features, especially close to (π, π) . This is pre-

cisely what is observed in experiment: large-momentum octet vectors are only observed at low frequencies. The reason why the large-momentum features appear only at low energies can be understood from Fig. 3, where the power spectrum along the Brillouin zone diagonal is compared for a single unitary pointlike scatterer with the power spectrum resulting from a single weak extended scatterer. Note that the intensity of the large-momentum peak, which results from the pointlike unitary scatterers, is almost frequency independent (see Fig. 3). However, its weight relative to the small-

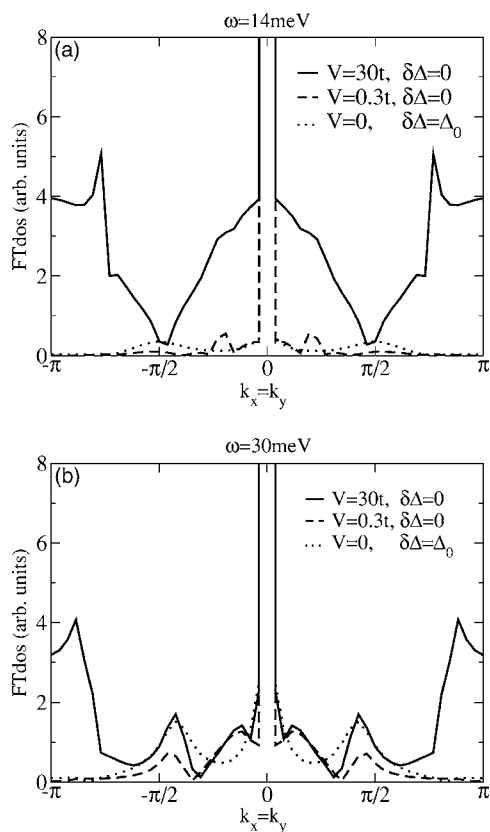


FIG. 3. Cut along the diagonal of the Brillouin zone ($k_x=k_y$) through the power spectrum of a strong pointlike τ_3 scatterer with $V_s=3.9$ eV (solid line), a weak extended τ_3 scatterer with $V_0=40$ meV, $\lambda=r_z=1.5$ (dashed line) and a pointlike τ_1 scatterer with $\delta\Delta=\Delta_0$ (dotted line) for an energy of (a) $\omega=14$ meV and (b) $\omega=30$ meV.

momentum features of the FTSTS signal decreases for large bias values. This occurs mainly because the intensity of the low momentum features, contributed by the weak scatterers, grows rapidly with frequency.

Overall, the power spectrum calculated within our realistic disorder model (sixth column in Fig. 2) reproduces the experimental one (seventh column in Fig. 2) qualitatively very well. This allows us to interpret some of the key features of the experimental power spectrum in the following way: (i) the dominant \mathbf{q}_1 peaks arise mainly from scattering by the order parameter modulations, i.e., by τ_1 scattering, (ii) the broadness of the \mathbf{q}_7 peaks, which are quite pronounced at small energies, is caused by poorly screened out-of-plane potential impurities, which act as extended τ_3 scatterers, (iii) the large momentum features at small frequencies originate from the in-plane native defects, which are modeled as pointlike unitary scatterers. Some discrepancies between our calculated and the experimental power spectrum certainly remain. The weight of the \mathbf{q}_1 peak is still too small in particular for small positive energies and the large momentum features in our calculation are arclike whereas the experiment observes discrete spots.

IV. CONCLUSIONS

We have suggested that a realistic model for the out-of-plane disorder in BSCCO-2212 should include: (i) order parameter inhomogeneities, which we have previously attributed to the fact that the oxygen dopant atoms modulate the pair interaction locally³² and which result in enhanced Andreev or τ_1 scattering, (ii) extended weak potential or τ_3 scatterers, which could originate, e.g., from the random substitution of Sr by Bi and which are spatially extended due to poor screening within the CuO_2 planes. In combination with the 0.2% in-plane native defects observed by the STM, which we model as pointlike unitary potential scatterers, our model for the out-of-plane disorder is able to reproduce the essential characteristics of the experimental Fourier transform patterns in BSCCO. The fact that the out-of-plane scatterers are spatially extended explains the absence of large-momentum octet peaks and the suppression of “background” features at higher energies. The large-momentum features at small energies are caused by the 0.2% pointlike strong in-plane scatterers. The \mathbf{q}_7 peaks are broadened considerably due to enhanced forward scattering caused by the spatially extended potential impurities. The τ_1 scattering, which arises from the order parameter inhomogeneities observed in BSCCO, strongly enhances the dispersive \mathbf{q}_1 peaks especially at higher energies. The reason why τ_1 scattering mostly contributes to \mathbf{q}_1 peaks is a simple consequence of the d -wave symmetry of the corresponding scattering matrix elements.

The agreement of the qualitative features of the power spectrum predicted by the model introduced in Ref. 32 for the out-of-plane O dopants with experiment is further evidence in support of the contention put forward there that the O defects in the BSCCO-2212 system are actually modulating the pair interaction g locally. Of course, comparisons of this type cannot directly determine the microscopic origin of the modulation of g , but since the experimental data with which we compare are from slightly overdoped samples, it seems unlikely that significant inhomogeneity is being driven by competition with a second order parameter. This therefore suggests that an atomic-scale modulation of electronic hopping parameters or electron-phonon coupling constants is indeed taking place in these materials near the dopant atoms.³²

ACKNOWLEDGMENTS

The authors acknowledge valuable conversations with W. A. Atkinson, A. V. Balatsky, J. C. Davis, J. Lee, and K. McElroy. We would especially like to thank J. C. Davis, J. Lee, and K. McElroy for sharing their data with us. We are grateful to A. Castro-Neto for bringing Ref. 33 to our attention. Partial support for this research (B.M.A., T.S.N., and P.J.H.) was provided by ONR N00014-04-0060. T.S.N. was supported by the A. v. Humboldt Foundation, and A.M. by the Institute for Fundamental Theory of the University of Florida.

- *Also at the Institut für Theoretische Physik, Freie Universität Berlin, Arnimallee 14, 14195 Berlin, Germany
- ¹A. Yazdani, C. M. Howald, C. P. Lutz, A. Kapitulnik, and D. M. Eigler, *Phys. Rev. Lett.* **83**, R176 (1999).
- ²E. W. Hudson, S. H. Pan, A. K. Gupta, K.-W. Ng, and J. C. Davis, *Science* **285**, 88 (1999).
- ³S. H. Pan, E. W. Hudson, K. M. Lang, H. Eisaki, S. Uchida, and J. C. Davis, *Nature (London)* **403**, 746 (2000).
- ⁴T. Cren, D. Roditchev, W. Sacks, J. Klein, J.-B. Moussy, C. Deville-Cavellin, and M. Laguës, *Phys. Rev. Lett.* **84**, 147 (2000).
- ⁵S.-H. Pan, J. P. O’Neal, R. L. Badzey, C. Chamon, H. Ding, J. R. Engelbrecht, Z. Wang, H. Eisaki, S. Uchida, A. K. Gupta, K.-W. Ng, E. W. Hudson, K. M. Lang, and J. C. Davis, *Nature (London)* **413**, 282 (2001).
- ⁶K. M. Lang, V. Madhavan, J. E. Hoffman, E. W. Hudson, H. Eisaki, S. Uchida, and J. C. Davis, *Nature (London)* **415**, 412 (2002).
- ⁷C. Howald, P. Fournier, and A. Kapitulnik, *Phys. Rev. B* **64**, 100504(R) (2001).
- ⁸J. E. Hoffman, E. W. Hudson, K. M. Lang, V. Madhavan, H. Eisaki, S. Uchida, and J. C. Davis, *Science* **295**, 466 (2002).
- ⁹C. Howald, H. Eisaki, N. Kaneko, and A. Kapitulnik, cond-mat/0201546 (unpublished).
- ¹⁰C. Howald, H. Eisaki, N. Kaneko, M. Greven, and A. Kapitulnik, *Phys. Rev. B* **67**, 014533 (2003).
- ¹¹E. W. Hudson, V. Madhavan, K. McElroy, J. E. Hoffman, K. M. Lang, H. Eisaki, S. Uchida, and J. C. Davis, *Physica B* **329**, 1365 (2003).
- ¹²K. McElroy, R. W. Simmonds, J. E. Hoffman, D.-H. Lee, J. Orenstein, H. Eisaki, S. Uchida, and J. C. Davis, *Nature (London)* **422**, 592 (2003).
- ¹³K. McElroy, D.-H. Lee, J. E. Hoffman, K. M. Lang, E. W. Hudson, H. Eisaki, S. Uchida, J. Lee, and J. C. Davis, cond-mat/0404005 (unpublished).
- ¹⁴N. Momono, A. Hashimoto, Y. Kobatake, M. Oda, and M. Ido, *J. Phys. Soc. Jpn.* **74**, 2400 (2005).
- ¹⁵P. Sprunger, L. Petersen, E. W. Plummer, E. Lægsgaard, and F. Besenbacher, *Science* **275**, 1764 (1997).
- ¹⁶J. Friedel, *Philos. Mag.* **43**, 153 (1952).
- ¹⁷D. Zhang and C. S. Ting, *Phys. Rev. B* **67**, 100506(R) (2003).
- ¹⁸Q.-H. Wang and D.-H. Lee, *Phys. Rev. B* **67**, 020511(R) (2003).
- ¹⁹B. M. Andersen and P. Hedegård, *Phys. Rev. B* **67**, 172505 (2003).
- ²⁰D. Zhang and C. S. Ting, *Phys. Rev. B* **69**, 012501 (2004).
- ²¹T. Pereg-Barnea and M. Franz, *Phys. Rev. B* **68**, 180506(R) (2003).
- ²²R. S. Markiewicz, *Phys. Rev. B* **69**, 214517(R) (2004).
- ²³U. Chatterjee, M. Shi, A. Kaminski, A. Kanigel, H. M. Fretwell, K. Terashima, T. Takahashi, S. Rosenkranz, Z. Z. Li, H. Raffy, A. Santander-Syro, K. Kadowaki, M. R. Norman, M. Randeria, and J. C. Campuzano, cond-mat/0505296 (unpublished).
- ²⁴K. McElroy, G.-H. Gweon, J. Graf, S. Y. Zhou, T. Sasagawa, H. Eisaki, H. Takagi, S. Uchida, D.-H. Lee, and A. Lanzara, *Phys. Rev. Lett.* **96**, 067005 (2006).
- ²⁵L. Capriotti, D. J. Scalapino, and R. D. Sedgewick, *Phys. Rev. B* **68**, 014508 (2003).
- ²⁶L. Zhu, W. A. Atkinson, and P. J. Hirschfeld, *Phys. Rev. B* **69**, 060503(R) (2004).
- ²⁷L. Dell’Anna, J. Lorenzana, M. Capone, C. Castellani, and M. Grilli, *Phys. Rev. B* **71**, 064518 (2005).
- ²⁸M. Cheng and W. P. Su, *Phys. Rev. B* **72**, 094512 (2005).
- ²⁹H. Eisaki, N. Kaneko, D. L. Feng, A. Damascelli, P. K. Mang, K. M. Shen, Z.-X. Shen, and M. Greven, *Phys. Rev. B* **69**, 064512 (2004).
- ³⁰G. Kinoda, H. Mashima, K. Shimizu, J. Shimoyama, K. Kishio, and T. Hasegawa, *Phys. Rev. B* **71**, 020502(R) (2005).
- ³¹K. McElroy, H. Eisaki, S. Uchida, and S. C. Davis, *Science* **309**, 1048 (2005).
- ³²T. S. Nunner, B. M. Andersen, A. Melikyan, and P. J. Hirschfeld, *Phys. Rev. Lett.* **95**, 177003 (2005).
- ³³H. Suhl, D. R. Fredkin, J. S. Langer, and B. T. Matthias, *Phys. Rev. Lett.* **9**, 62 (1962).
- ³⁴A. I. Larkin, *Sov. Phys. JETP* **31**, 784 (1970).
- ³⁵I. N. Khlyustikov and A. I. Buzdin, *Adv. Phys.* **36**, 271 (1987).
- ³⁶Y. He, T. S. Nunner, P. J. Hirschfeld, and H.-P. Cheng, cond-mat/0601157 (unpublished).
- ³⁷R. Raimondi, J. H. Jefferson, and L. F. Feiner, *Phys. Rev. B* **53**, 8774 (1996).
- ³⁸E. Pavarini, I. Dasgupta, T. Saha-Dasgupta, O. Jepsen, and O. K. Andersen, *Phys. Rev. Lett.* **87**, 047003 (2001).
- ³⁹M. C. Aronson, S. B. Dierker, B. S. Dennis, S.-W. Cheong, and Z. Fisk, *Phys. Rev. B* **44**, 4657–4660 (1991).
- ⁴⁰A. Ghosal, A. Kopp, and S. Chakravarty, *Phys. Rev. B* **72**, 220502(R) (2005).
- ⁴¹A. C. Fang, L. Capriotti, D. J. Scalapino, S. A. Kivelson, N. Kaneko, M. Greven, and A. Kapitulnik, *Phys. Rev. Lett.* **96**, 017007 (2006).
- ⁴²J.-X. Zhu, cond-mat/0508646 (unpublished).
- ⁴³J. Lee, K. McElroy, J. Slezak, S. Uchida, H. Eisaki, and J. C. Davis, *Bull. Am. Phys. Soc.* **50**, 299, (2005).
- ⁴⁴Jian-Xin Zhu, K. McElroy, J. Lee, T. P. Devereaux, Qimiao Si, J. C. Davis, A. V. Balatsky, cond-mat/0507621.
- ⁴⁵B. M. Andersen, A. Melikyan, T. S. Nunner, and P. J. Hirschfeld, *Phys. Rev. Lett.* **96**, 097004 (2006).
- ⁴⁶T. S. Nunner and P. J. Hirschfeld, *Phys. Rev. B* **72**, 014514 (2005).
- ⁴⁷M. R. Norman, M. Randeria, H. Ding and J. C. Campuzano, *Phys. Rev. B* **52**, 615 (1994).
- ⁴⁸Note we use the term “power spectrum” for the square root of the conventional definition.